LBL-11818

Lawrence Berkeley Laboratory
UNIVERSITY OF CALIFORNIA

Invited speaker at the Workshop on "Future Relativistic Heavy Ion Experiments", GSI Darmstadt, West Germany, October 7-10, 1980

THE HISS SPECTROMETER AT LBL

D. Greiner

November 1980

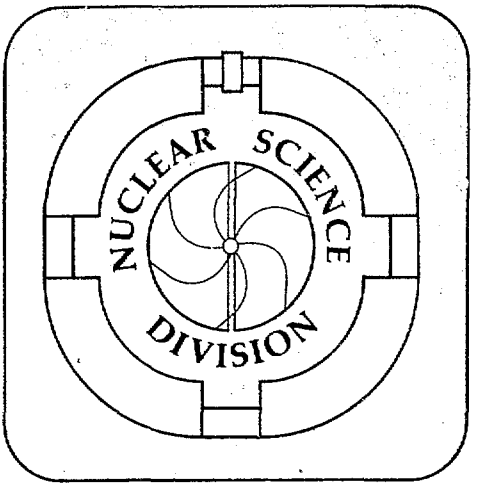

Prepared for the U.S. Department of Energy under Contract W-7405-ENG-48

LBL-11818

The HISS Spectrometer at LBL

D. Greiner

Nuclear Science Division
Lawrence Berkeley Laboratory
University of California
Berkeley, CA 94720

This work was supported by the Division of Nuclear Physics of the Office of High Energy and Nuclear Physics of the U.S. Department of Energy under Contract W-7405-ENG-48.

(Talk given at Workshop on "Future Relativistic Heavy Ion Experiments" held at GSI Darmstadt, October 7-10, 1980)

The Heavy Ion Spectrometer System at LBL is designed to be a general purpose experimental work bench able to support a wide variety of experiments. Our philosophy is to provide instruments capable of investigating, with multi-particle sensitivity, a large portion of phase space. We have not chosen a particular region such as mid-rapidity or projectile frame but, instead, have made sure that the magnet and the instrumentation allow these choices as well as many others. In fig. 1 are shown the beam line and the HISS magnet. The beam can be brought into the magnet at a variable position and the magnet can be rotated. This allows a wide range of experiments; some possible configurations will be shown later. The high dispersion beam line, to be added in 1982, allows the use of clean beams of unstable particles. These beams would be secondary beams produced upstream near the exit of the Bevatron. The resolution of this line can deliver, for instance, a pure beam of ^{55}Fe produced from a ^{56}Fe primary beam.

The first experiments to be run on HISS will use the phase I detector system shown in figure 2. These detectors consist of drift chambers to measure trajectories, Xe ionization chamber for charge, and a time-of-flight wall to measure the mass of the particles. There is also some change measuring capability in the drift chambers, one plane of wires is pulse height analyzed allowing charge 1 and 2 to be distinguished. This phase 1 system covers a rather small solid angle as shown in a typical configuration in figure 3. A larger array planed for phase II was shown by Howel Pugh earlier. All these detectors have been designed to operate over the dynamic range necessary to make full use of the heavy beams which will be available from the upgraded Bevalac in 1982.

I will now go into some details about these detectors: The drift chamber design is shown in figure 4. There are two planes of wires offset by 1 cm per measurement direction. This allows resolution of the left-right ambiguity. The use of 3 measurement directions allows detection of multiple tracks. Because the chambers are rather thick, we are able to produce a direction vector for each track. This vector points with an accuracy of ≈ 3mm to the expected position in the next chamber thus greatly simplifying the trajectory reconstruction. A primary difficulty with relativistic heavy ions in gaseous detectors is the production of spurious tracks by δ rays; we have overcome this problem by designing electronics which selects the largest pulse in the drift region for digitization.

The Ze ionization chamber or what we have come to call the MUltiple Sample Ionization Chamber is shown in figure 5. The ionization cloud produced by a particle is drifted down to a set of 50 anodes where their time of arrival and pulse height are digitized using electronics developed by the TPC project at LBL. In figure 6 is shown a calculated distribution of these pulse heights for many tracks in a single cell. We see from this curve that the best resolution is on the low energy side of the peak. Figure 7 shows the pulse heights returned for a single ^{56}Fe track through the chamber. There are many possible algorithms to extract the charge of the particle. We have been exploring simple methods which yield sufficient resolution and are amenable to calculation in hardware or on fast micros for preprocessing of event data. The result of one such method is shown in figure 8. The method used there involves ordering the pulse heights and then averaging the sixth through twentieth signals. As can be seen from the figure we can clearly resolve Z = 25 and 26. We will verify these predictions with the phase I chamber in January 1981.

The time of flight wall is made up of 30 scintillators each 10 x 4 x 200 cm viewed by photomultiplier tubes on each end. This is a rather standard system. The results for a test of a single module are shown in figure 9 where a resolution of 210 PS (FWHM) was achieved for ^{12}C at 2.1 Gev/nuc.

Now I would like to show a few examples of the different configurations of these detectors at HISS to demonstrate the wide variety of experiments made possible by the system.

Figures 10, 11, 12 and 13 show arrangements which respectively can measure: large angle production, high transverse momentum production, pair production and 180° correlations. This is not an exhaustive list.

There are five phase 1 experiments which are approved by the PAC to run on HISS. A summary of the goals of these five is shown in figure 14. I will not elaborate on these here except to point out that a strong effort will be made to run these experiments before the July 1981 shutdown to improve Bevalac vacuum.

Now I would like to demonstrate the use of HISS in a specific experiment. The first experiment is an investigation of the exclusive states produced in the fragmentation of ^{12}C. I want to investigate the possibility of observing the long-lived states suggested earlier by Friedlander and Heckman. A summary of their observations is shown in figure 15. Certain explanations of their results would predict that the diproton state exists. The exercise then is to see if this state can be seen in ^{12}C fragmentation at the 6% level. We assume the reaction is dominated by direct processes with a 6% production via a resonant state as shown in figure 16. The basic difficulty is illustrated in figure 17; particles which decay down stream of the target may cause distortion of the signature sufficient to mask detection. The only indication of the point of decay comes from the slope of the trajectory in the vertical direction where it is unaffected by the magnetic field of the HISS dipole. Figure 18 shows the invariant mass

spectra for 10000 Monte Carlo generated events. There is visible even in this un-cut data a slight enhancement at the mass (2062 Mev) assumed for the di-proton. If we look at the proton production distance from the target (Fig. 19) we see that, though the resolution is poor, there is a definite tail towards the downstream region. From the next figure 20 we see that requiring the proton pairs originate downstream from the target greatly enhances the effect and a definite resonance structure can be seen in the effective mass distribution. By applying a more stringent cut (Fig. 21) requiring production 5 to 70 cm past the target we can produce an almost pure spectra of diprotons. Using the distribution of these distances in fig. 22 an estimate of the lifetime can be obtained which is close to the value used in generation of the sample. This has been a rather easy test; let's make it harder. With $^{12}C \rightarrow {}^{10}Be + p + p$ we had no combinational background to obscure the resonant state. We add this background by mixing direct plus resonance of production with direct production. The case selected is the final state $^{9}Li + p + p + p$; we let the reaction be 94% direct ^{12}C $^{9}Li + p + p$ and mix 6% direct and resonance $^{12}C \rightarrow {}^{9}Li + p + dp$ (2062) and generate 10000 events. Fig. 23 shows the uncut invariant mass which again shows a slight enhancement. Cutting for only downstream produced pairs (Fig. 24) gives a little larger hump. Finally a series of cuts shown in Fig. 25 removes a large part of the background.

I have gone through this exercise to show that the HISS system has the ability to detect long-lived states. There are many other things that will be done with the apparatus. I hope this talk will provide a stimulus for people to think up other and better experiments.

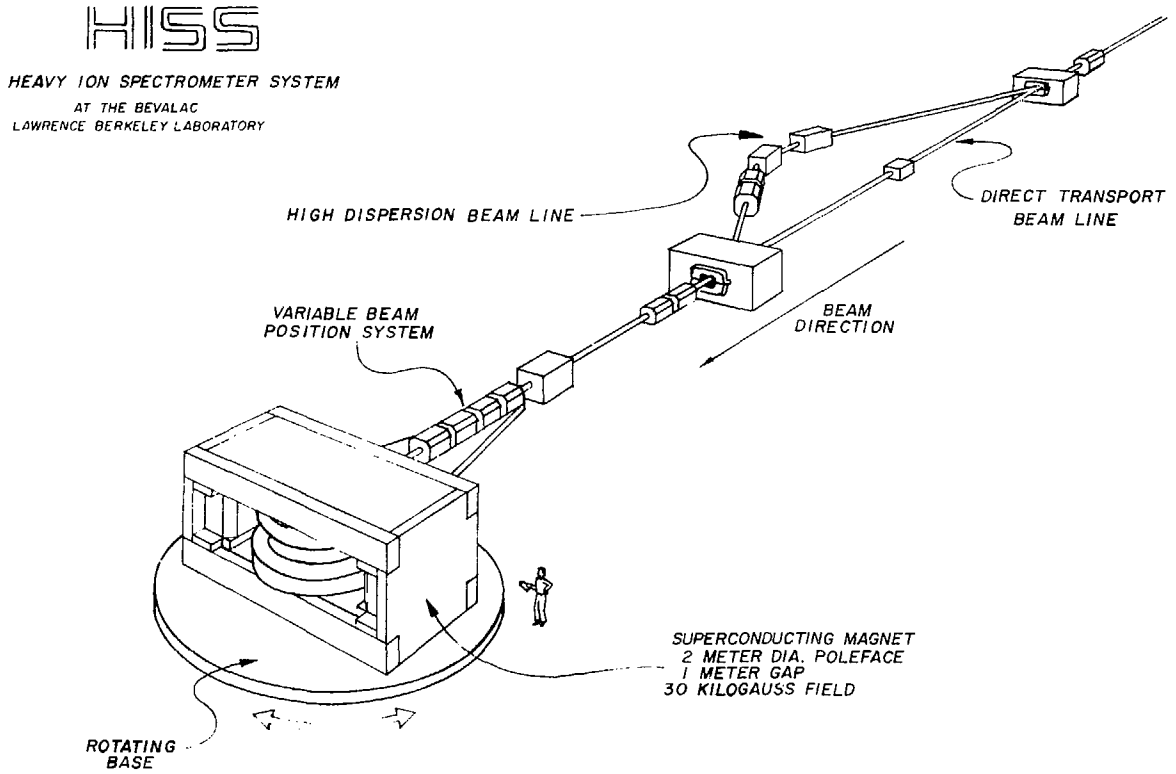

Figure 1.

XBL 799-12037

PARTICLE IDENTIFICATION AT HISS

For multi particle events we must determine:

Momentum — Trace trajectory using drift chambers

Charge — dE/dx in Xenon ionization chamber

Mass — Time of flight

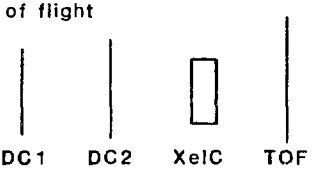

PHASE 1 INSTRUMENTATION

DETECTOR	CHARACTERISTICS	FUNDING
DRIFT CHAMBERS	2 chambers, 3 planes each 1m x 2m, resolution $\leq 300\mu$ $\Delta p \sim 2.5A$	electronics, mech parts--LBL machining--UCLA
XENON IONIZATION CHAMBER	1m x 1m x 50 cm $\Delta Z/Z \leq .01$	electronics, gas system--LBL detector--UC Davis
TOF WALL	2m x 3m $\Delta A \sim .03A$	electronics--LBL plastic--INS (Japan) (positioning devices--LSU)

Figure 2.

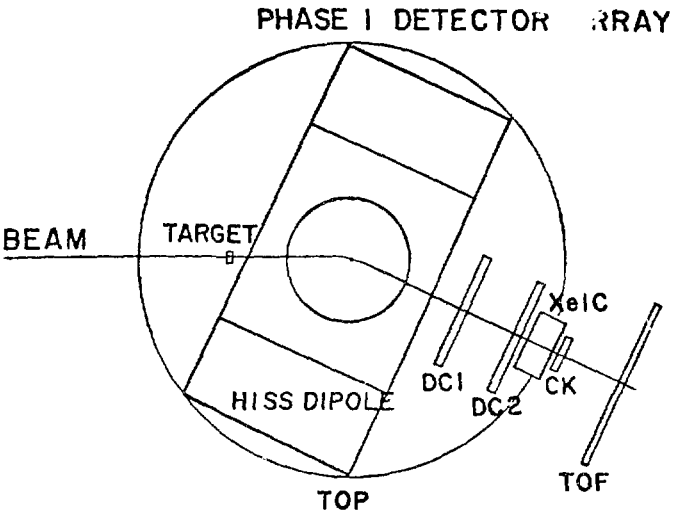
PHASE I DETECTOR ARRAY
BEAM
TARGET
HISS DIPOLE
DC1
DC2
XeIC
CK
TOF
TOP

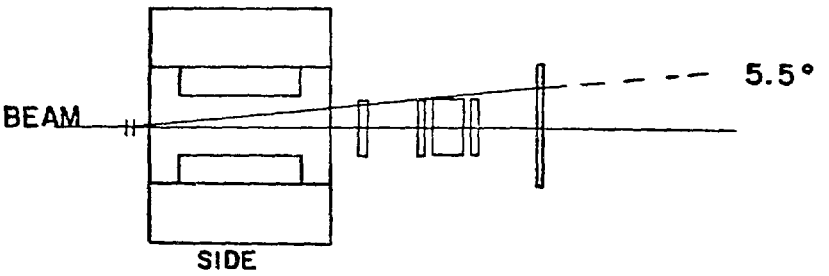
BEAM
5.5°
SIDE

Figure 3.

HISS DRIFT CHAMBER

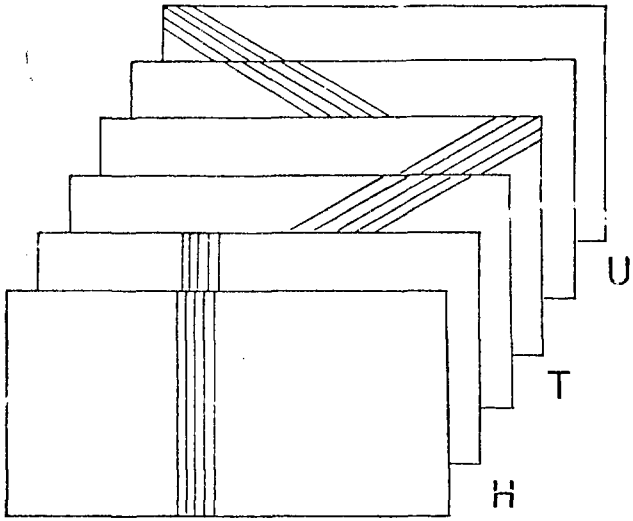

WIRE ORIENTATION

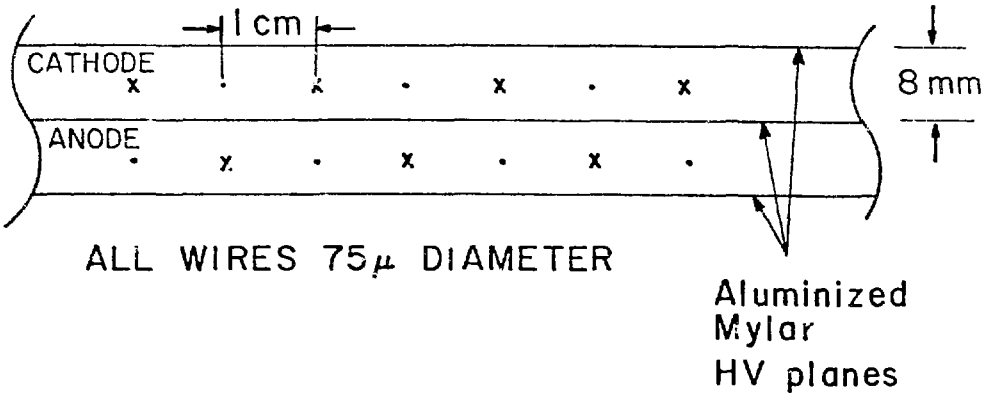

ALL WIRES 75μ DIAMETER

TYPICAL CROSS SECTION

Figure 4.

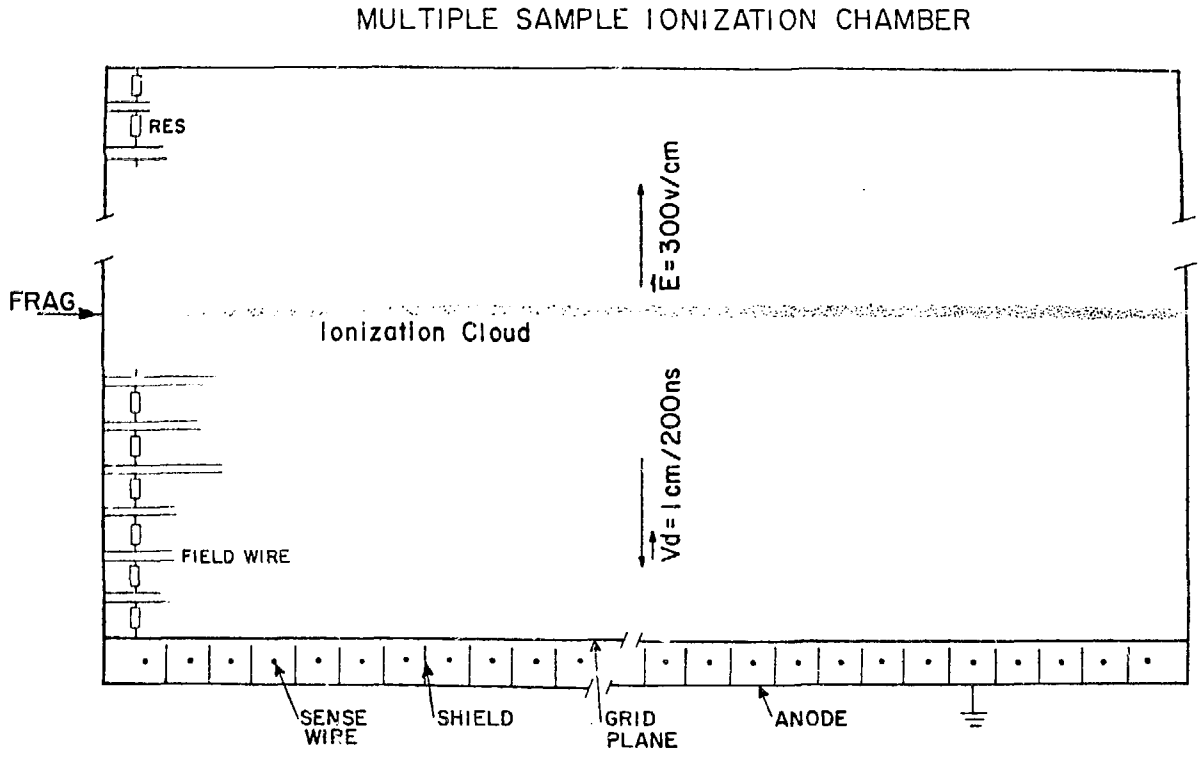
MULTIPLE SAMPLE IONIZATION CHAMBER
RES
E = 300v/cm
FRAG
Ionization Cloud
Vd = 1cm/200ns
FIELD WIRE
SENSE WIRE
SHIELD
GRID PLANE
ANODE

Figure 5.

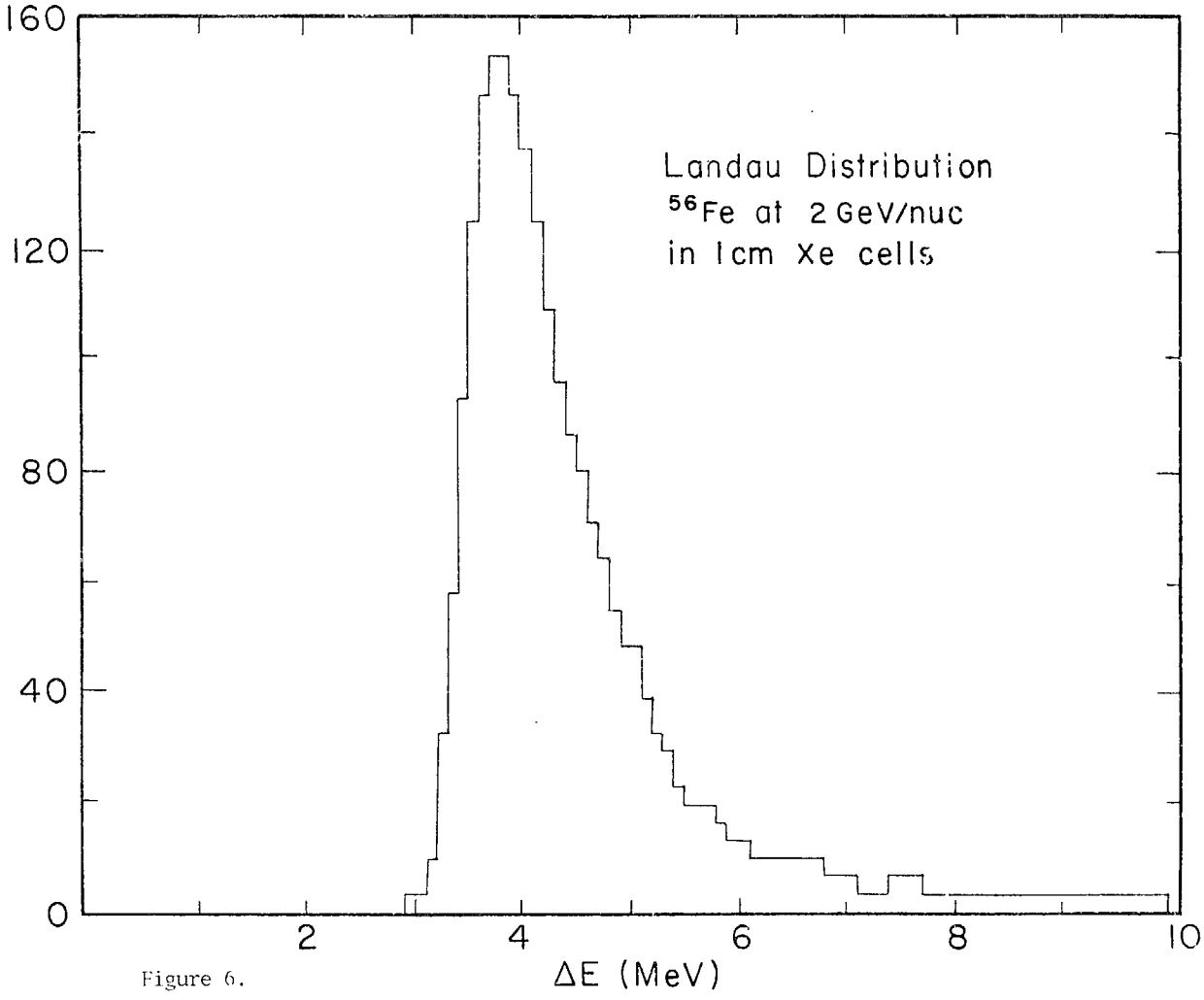
Landau Distribution
56Fe at 2 GeV/nuc
in 1cm Xe cells
160
120
80
40
0
2
4
6
8
10
ΔE (MeV)

Figure 6.

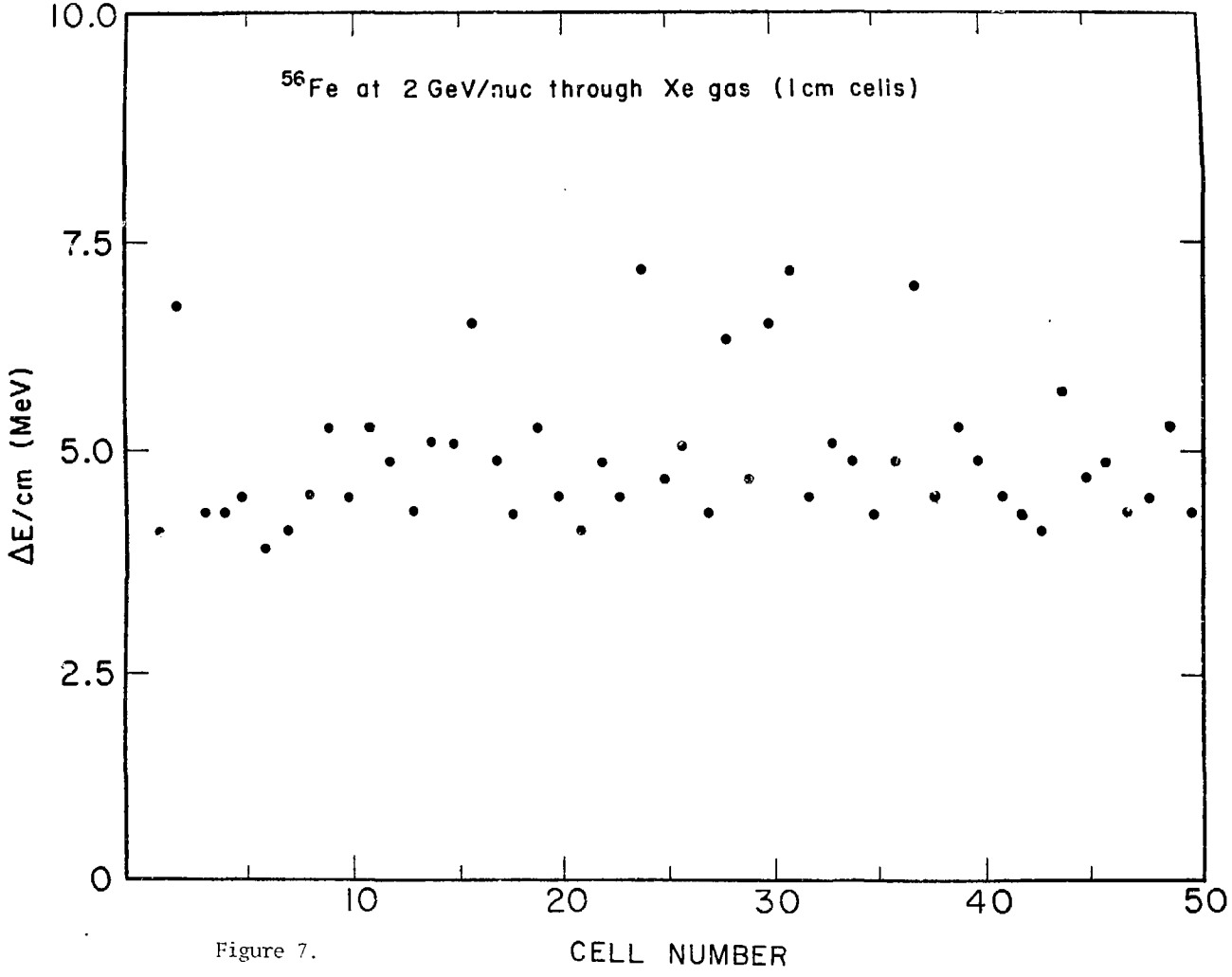
10.0
7.5
5.0
2.5
0
ΔE/cm (MeV)
56Fe at 2 GeV/nuc through Xe gas (1cm cells)
10
20
30
40
50
CELL NUMBER

Figure 7.

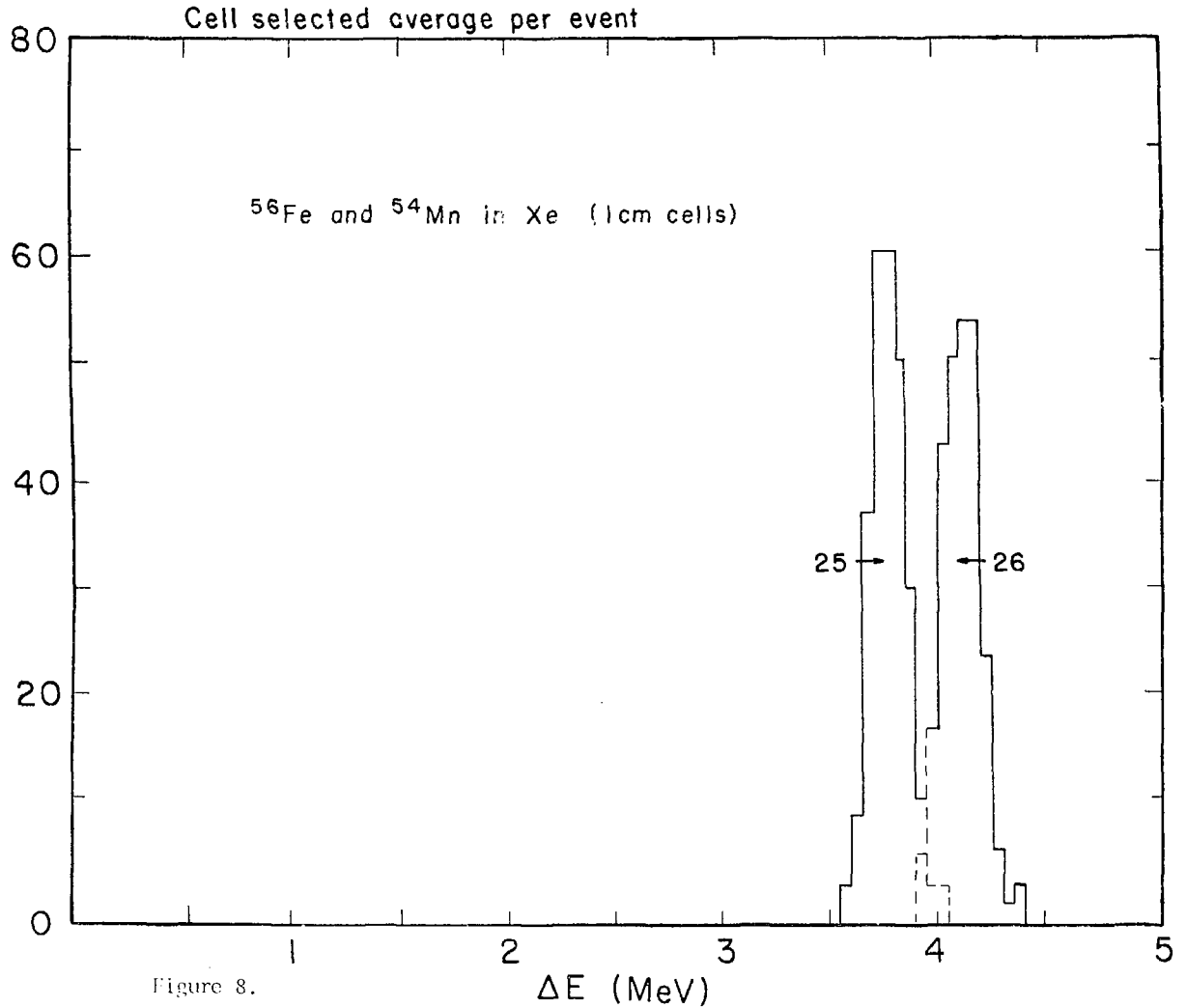
Cell selected average per event
^{56}Fe and ^{54}Mn in Xe (1cm cells)
25
26
80
60
40
20
0
1
2
3
4
5
ΔE (MeV)

Figure 8.

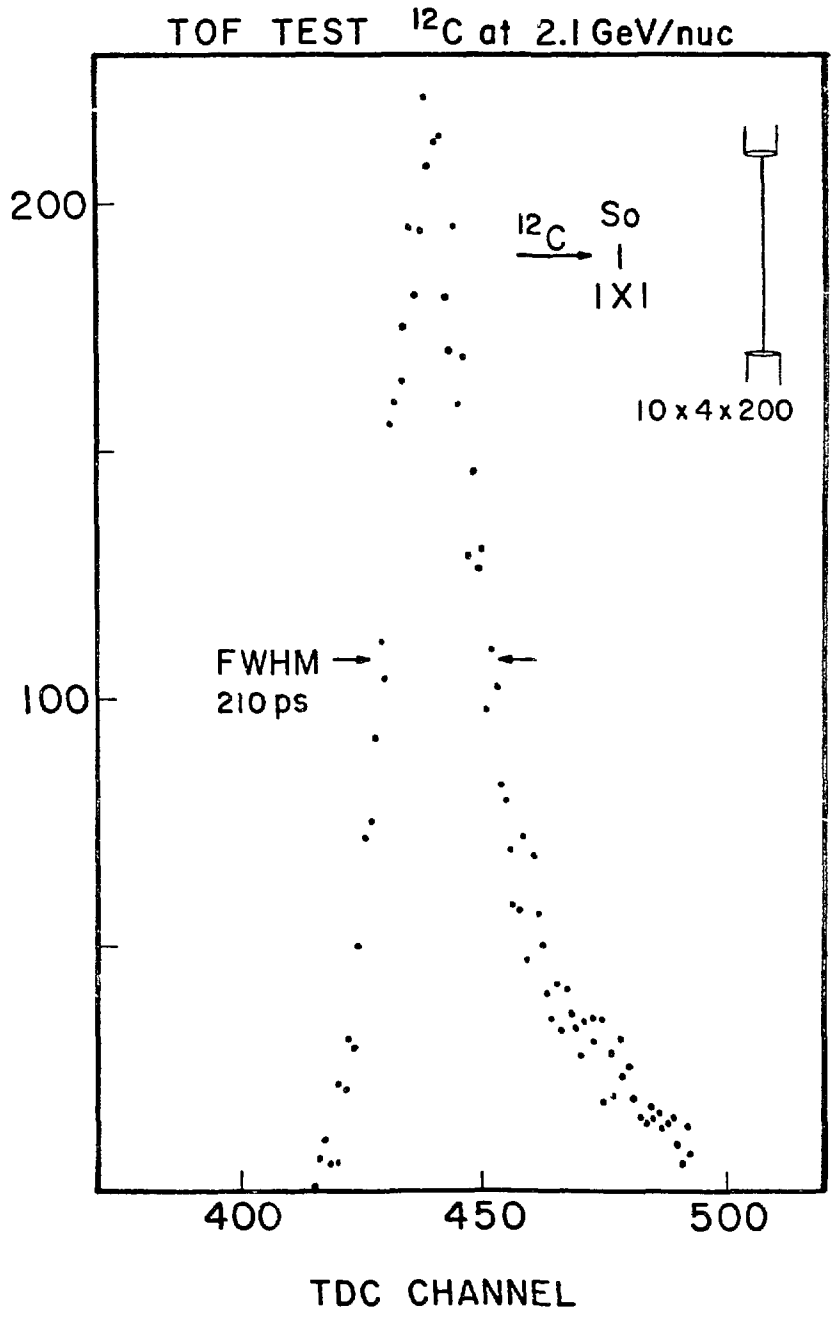
TOF TEST ^{12}C at 2.1 GeV/nuc
200
100
^{12}C
So
1
1X1
10 x 4 x 200
FWHM
210 ps
400
450
500
TDC CHANNEL

Figure 9.

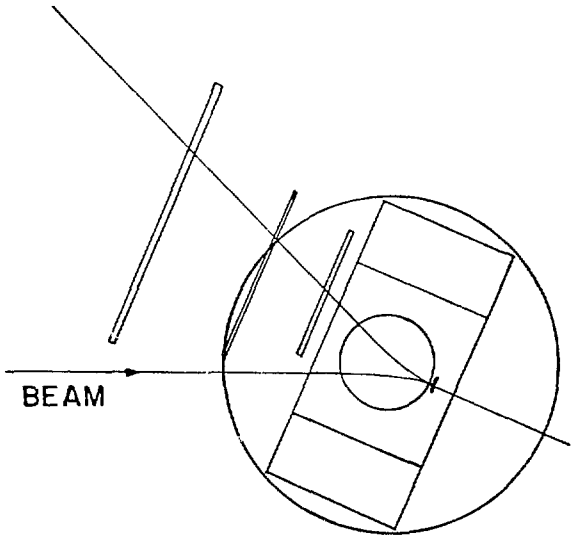

Figure 10.

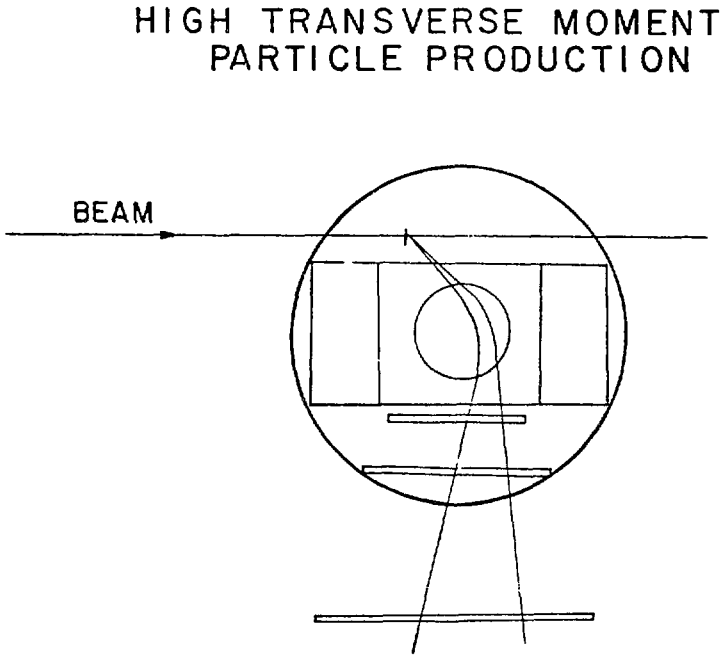

Figure 11.

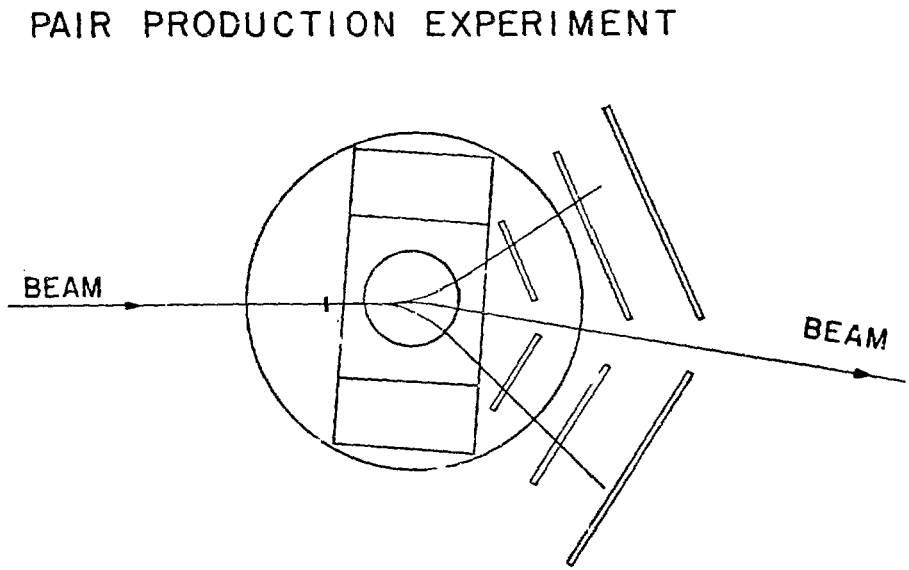

Figure 12.

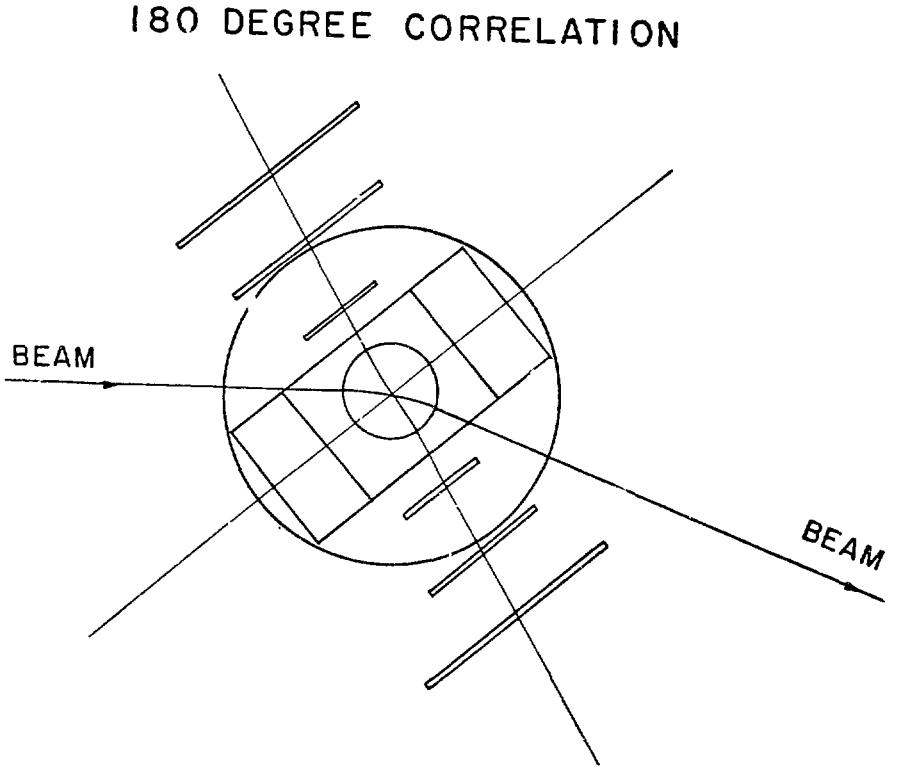

Figure 13.

HISS PHASE I EXPERIMENTS

COULOMB DISSOCIATION OF $^{16,18}O$--LLL, SSL, LBL

GOALS: EXCITATION OF GIANT RESONANCES IN $^{16,18}O$ DECAY

INVARIANT MASS SPECTRA FROM ^{12}C--LSU, SSL, UCD, NRL, LBL

GOALS: EXCITATION SPECTRA FROM EXCLUSIVE MODES
SEARCH FOR STRUCTURE IN INVARIANT MASS SPECTRA

FRAGMENTATION OF ^{56}FE--SSL, NRL, LBL

GOALS: SEARCH FOR COLLECTIVE EFFECTS EVIDENCED BY STRUCTURE IN INVARIANT MASS SPECTRA

MEASUREMENTS OF LARGE P_T FRAGMENTS--INS, LBL

GOALS: STUDY COLLECTIVE EFFECTS NEAR KINEMATIC LIMIT AND THE ASSOCIATED MULTIPLICITIES

TWO PARTICLE CORRELATIONS AT SMALL ΔP--UCLA, UCD, LBL

GOALS: USE SECOND ORDER INTERFERENCE BETWEEN IDENTICAL PARTICLES TO DETERMINE INTERACTION VOLUME AND TIME

Figure 14.

DATA OF FRIEDLANDER ET AL. ARE CONSISTENT WITH:

1. 6% OF FRAGMENTS ARE ANOMALOUS.
2. THEIR CROSS SECTION IS LARGE.
3. THEIR LIFETIME IS > 30 CM (AT 2.1 GEV/NUC).

WE ASSUME A STATE IS PRODUCED WITH DEFINITE MASS AND A LIFETIME OF 30 CM IN THE LABORATORY.

SPECIFIC CASE:

$$^{12}C \rightarrow {}^{10}BE + DP\ (2062)$$

$$\hookrightarrow P + P$$

MIXED WITH 94% PURE DIRECT REACTION

$$^{12}C \rightarrow {}^{10}BE + P + P$$

Figure 15.

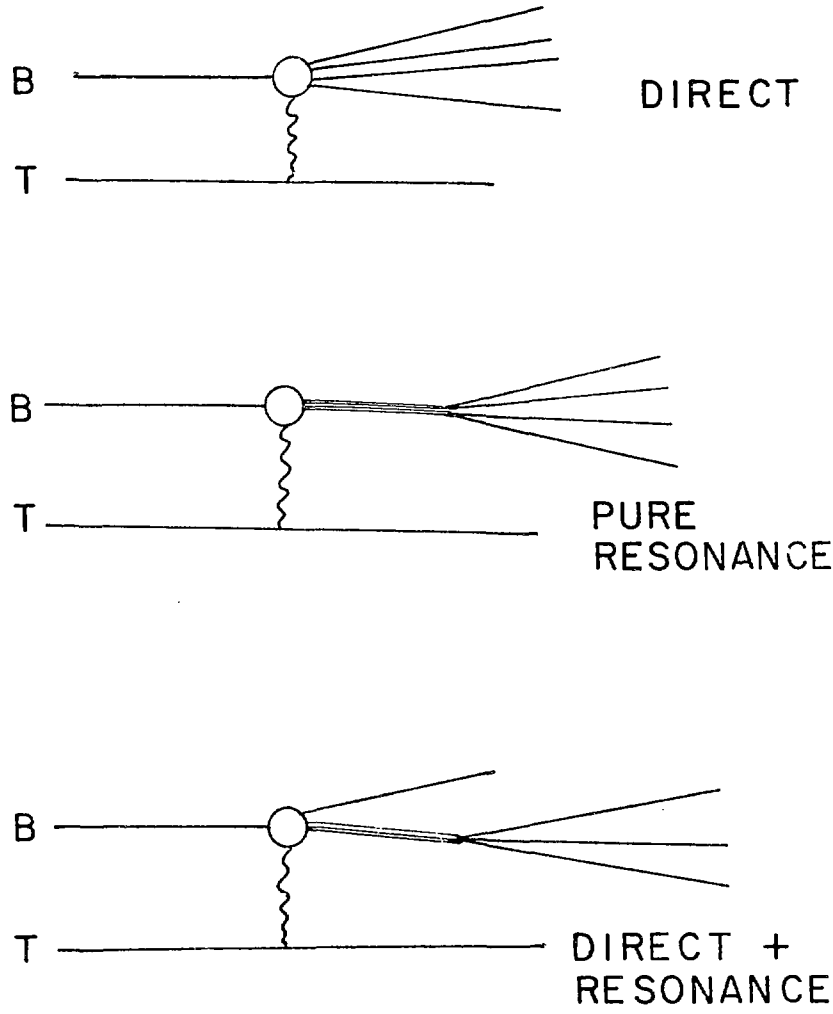

Figure 16.

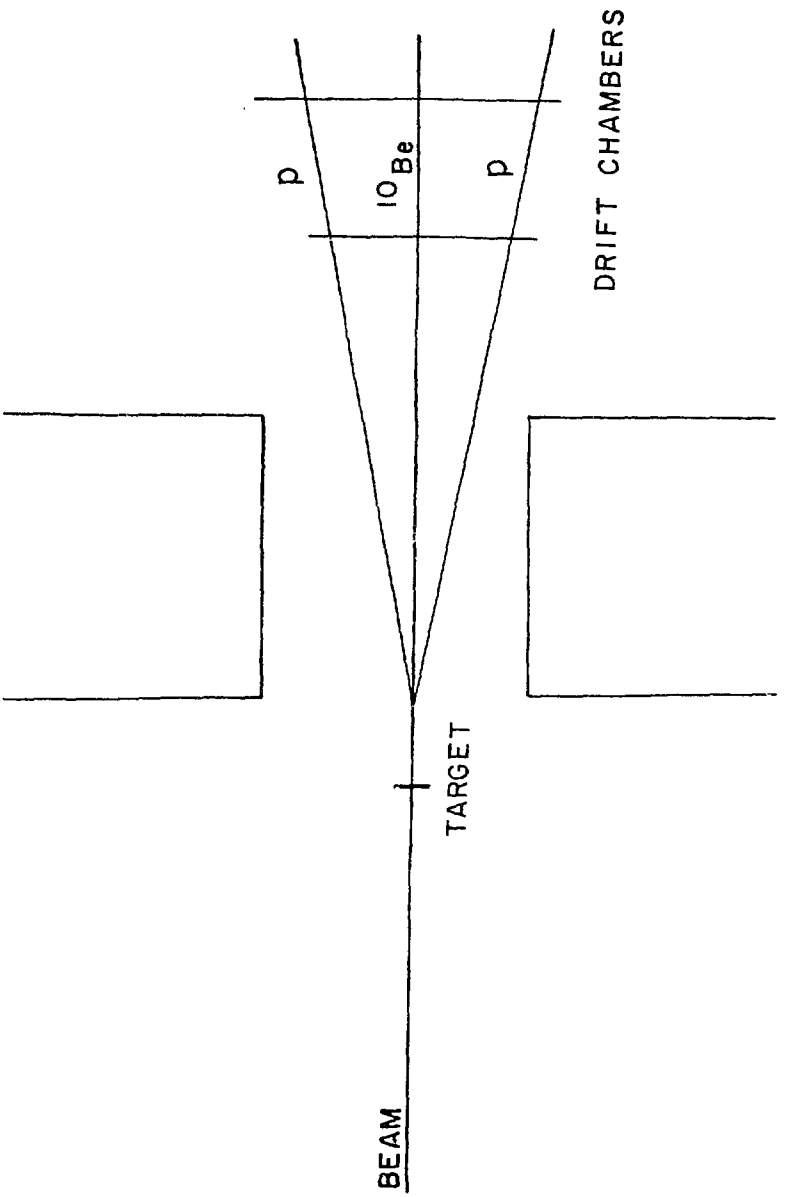

Figure 17.

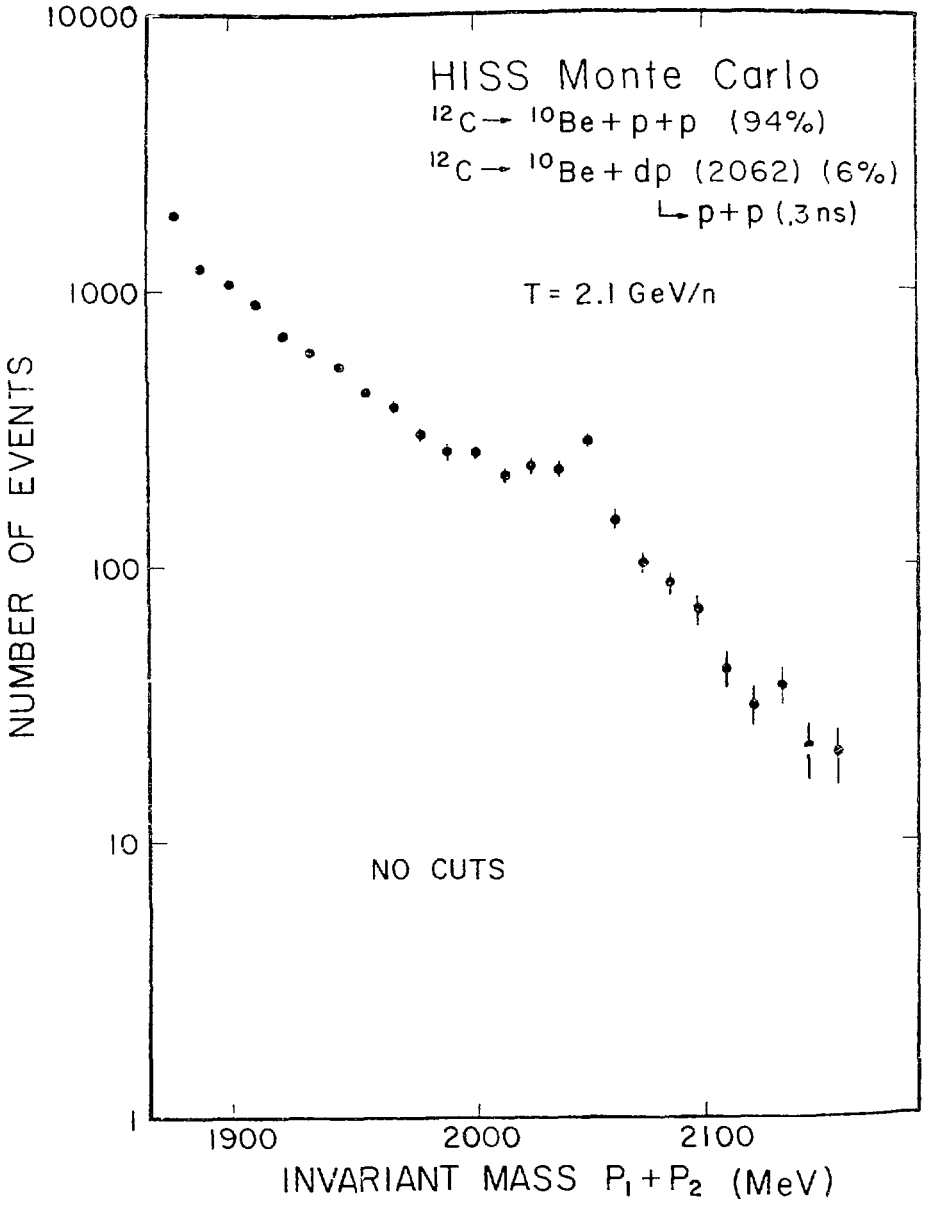
HISS Monte Carlo
$^{12}C \rightarrow {}^{10}Be + p + p$ (94%)
$^{12}C \rightarrow {}^{10}Be + dp$ (2062) (6%)
$\hookrightarrow p + p$ (.3 ns)
T = 2.1 GeV/n
NO CUTS
NUMBER OF EVENTS
10000
1000
100
10
1
1900
2000
2100
INVARIANT MASS $P_1 + P_2$ (MeV)

Figure 18.

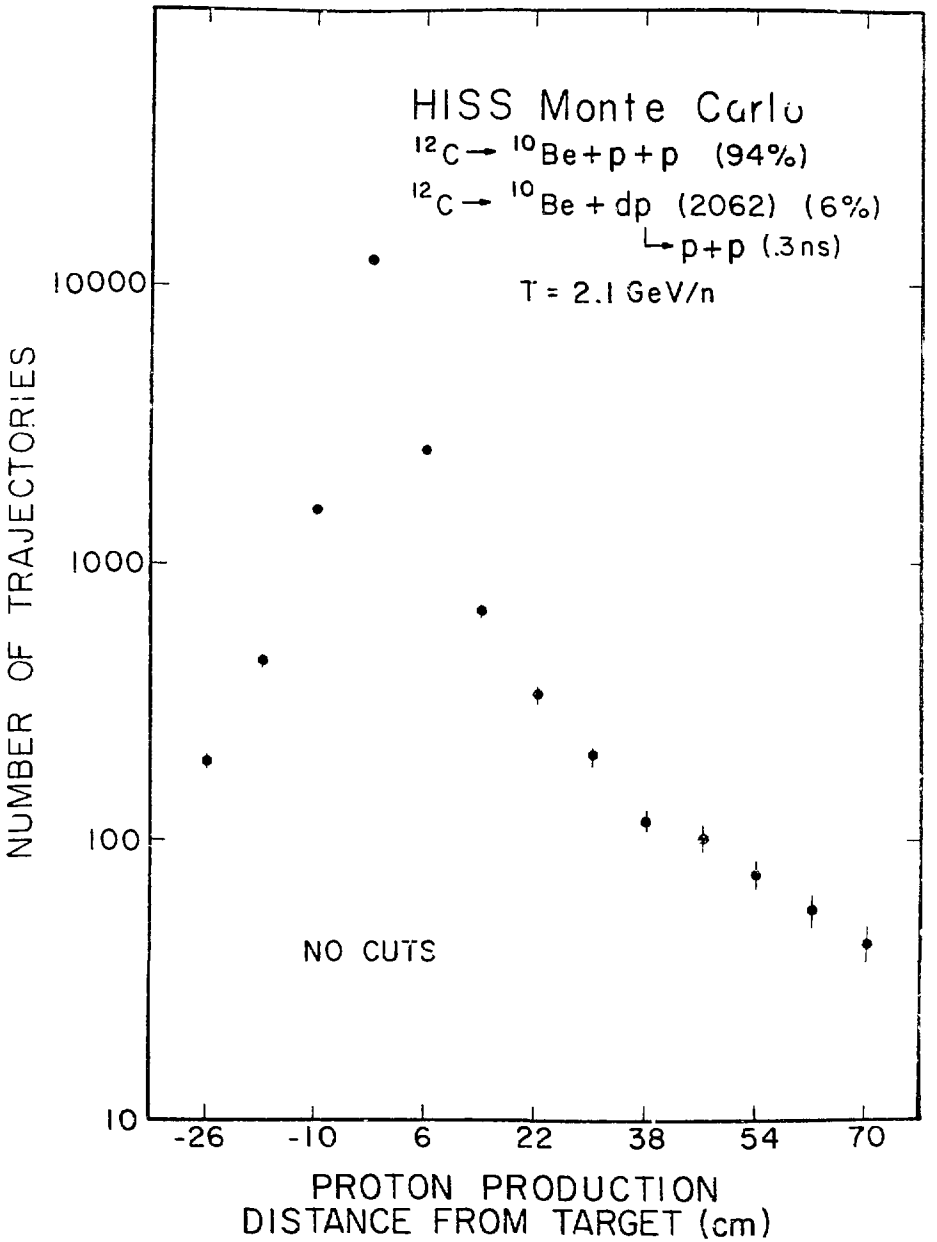
HISS Monte Carlo
$^{12}C \rightarrow {}^{10}Be + p + p$ (94%)
$^{12}C \rightarrow {}^{10}Be + dp$ (2062) (6%)
$\hookrightarrow p + p$ (.3ns)
T = 2.1 GeV/n
NUMBER OF TRAJECTORIES
10000
1000
100
10
NO CUTS
-26
-10
6
22
38
54
70
PROTON PRODUCTION
DISTANCE FROM TARGET (cm)

Figure 19.

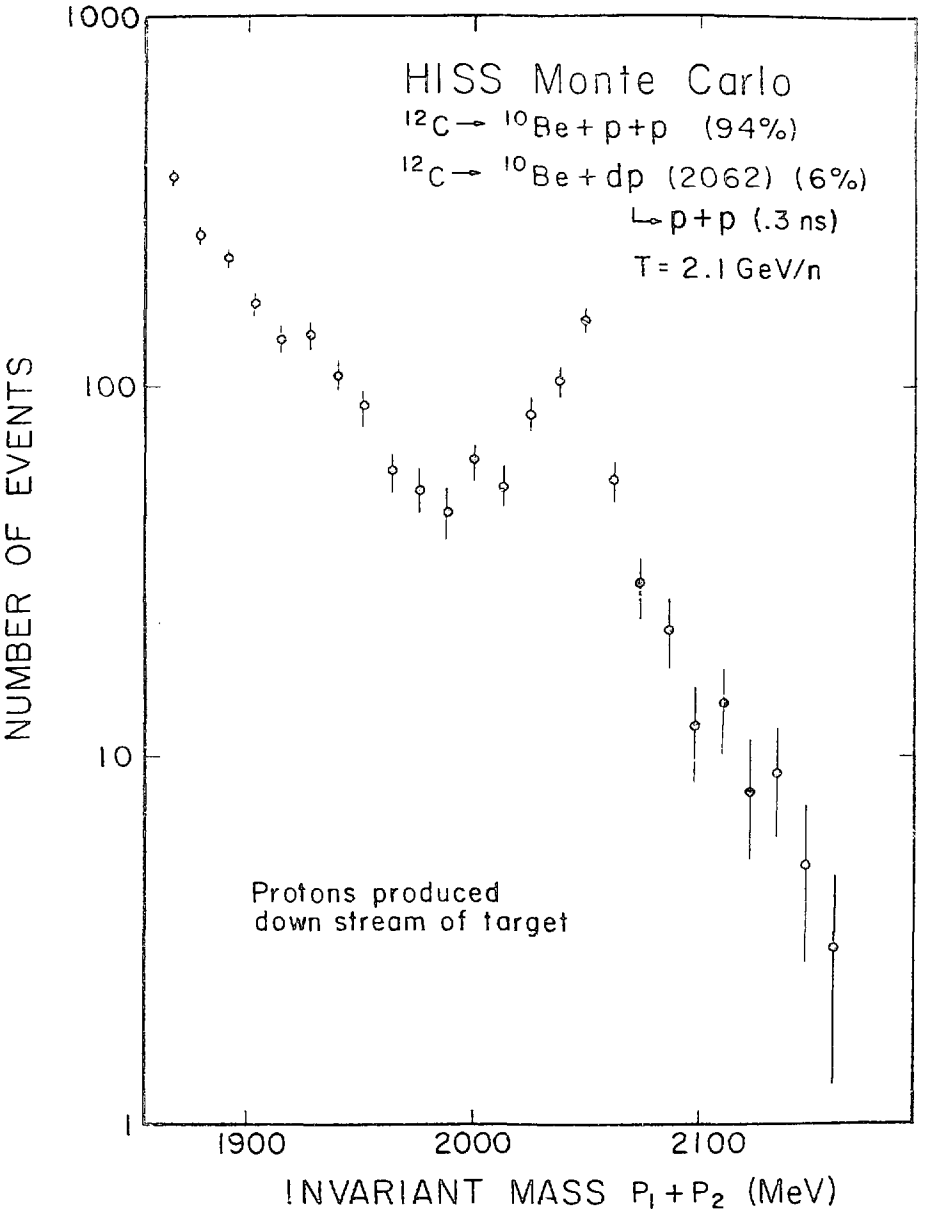
HISS Monte Carlo
$^{12}C \rightarrow {}^{10}Be + p + p$ (94%)
$^{12}C \rightarrow {}^{10}Be + dp$ (2062) (6%)
$\hookrightarrow p + p$ (.3 ns)
T = 2.1 GeV/n
Protons produced
down stream of target
NUMBER OF EVENTS
1000
100
10
1
1900
2000
2100
INVARIANT MASS $P_1 + P_2$ (MeV)

Figure 20.

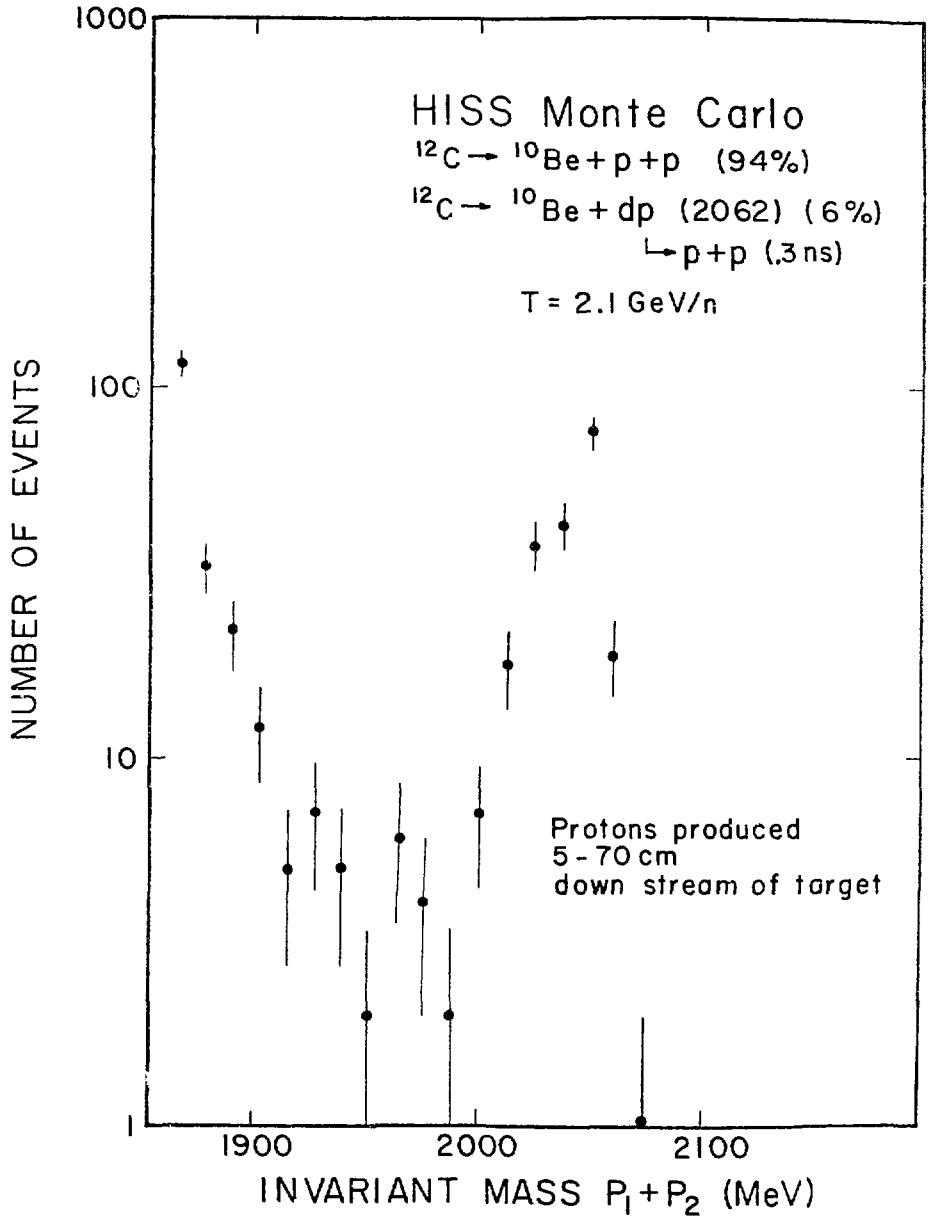
HISS Monte Carlo
$^{12}C \rightarrow {}^{10}Be + p + p$ (94%)
$^{12}C \rightarrow {}^{10}Be + dp$ (2062) (6%)
$\hookrightarrow p + p$ (.3 ns)
T = 2.1 GeV/n
Protons produced
5 - 70 cm
down stream of target
NUMBER OF EVENTS
1000
100
10
1
1900
2000
2100
INVARIANT MASS $P_1 + P_2$ (MeV)

Figure 21.

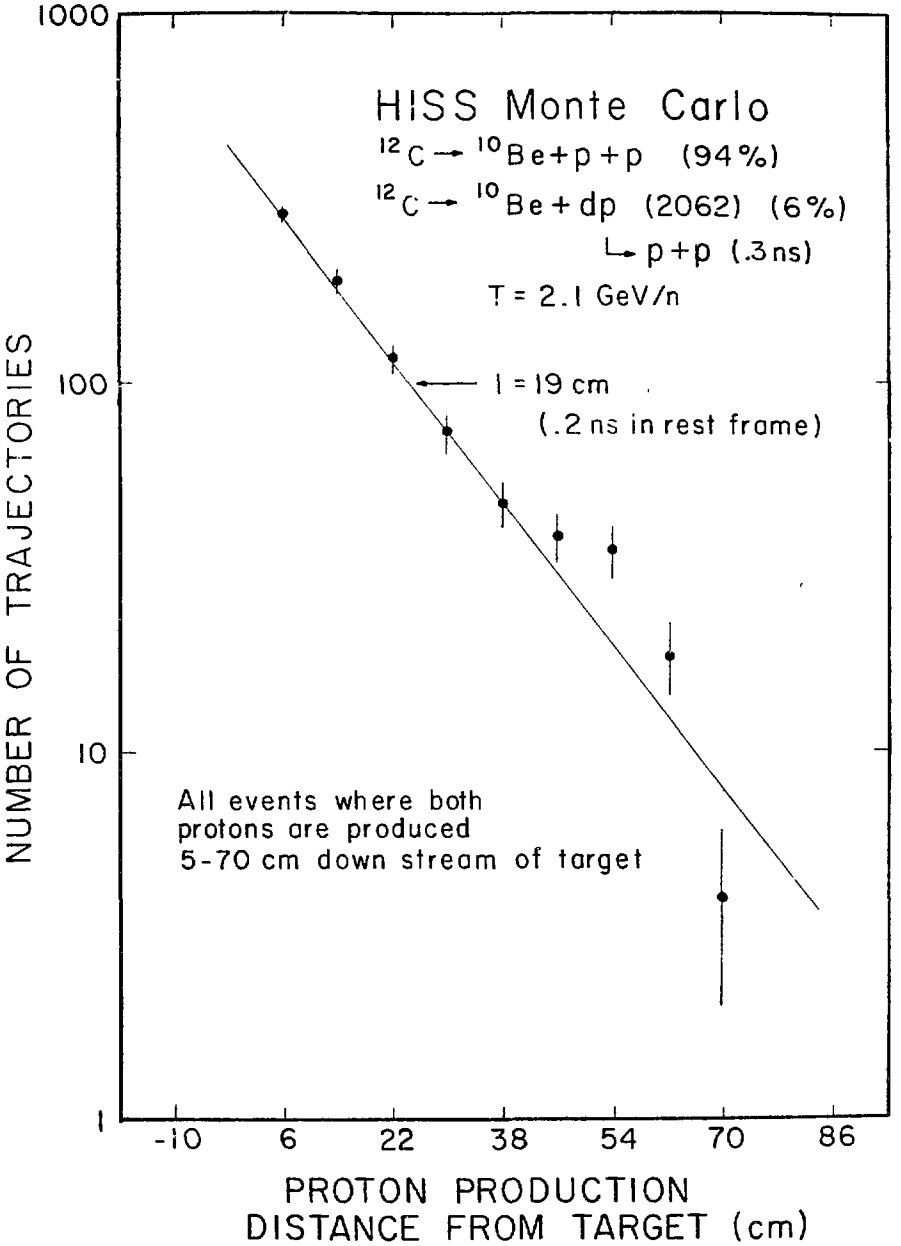
HISS Monte Carlo
$^{12}C \rightarrow {}^{10}Be + p + p$ (94%)
$^{12}C \rightarrow {}^{10}Be + dp$ (2062) (6%)
$\hookrightarrow p + p$ (.3 ns)
T = 2.1 GeV/n
l = 19 cm
(.2 ns in rest frame)
All events where both
protons are produced
5-70 cm down stream of target
NUMBER OF TRAJECTORIES
1000
100
10
1
-10
6
22
38
54
70
86
PROTON PRODUCTION
DISTANCE FROM TARGET (cm)

Figure 22.

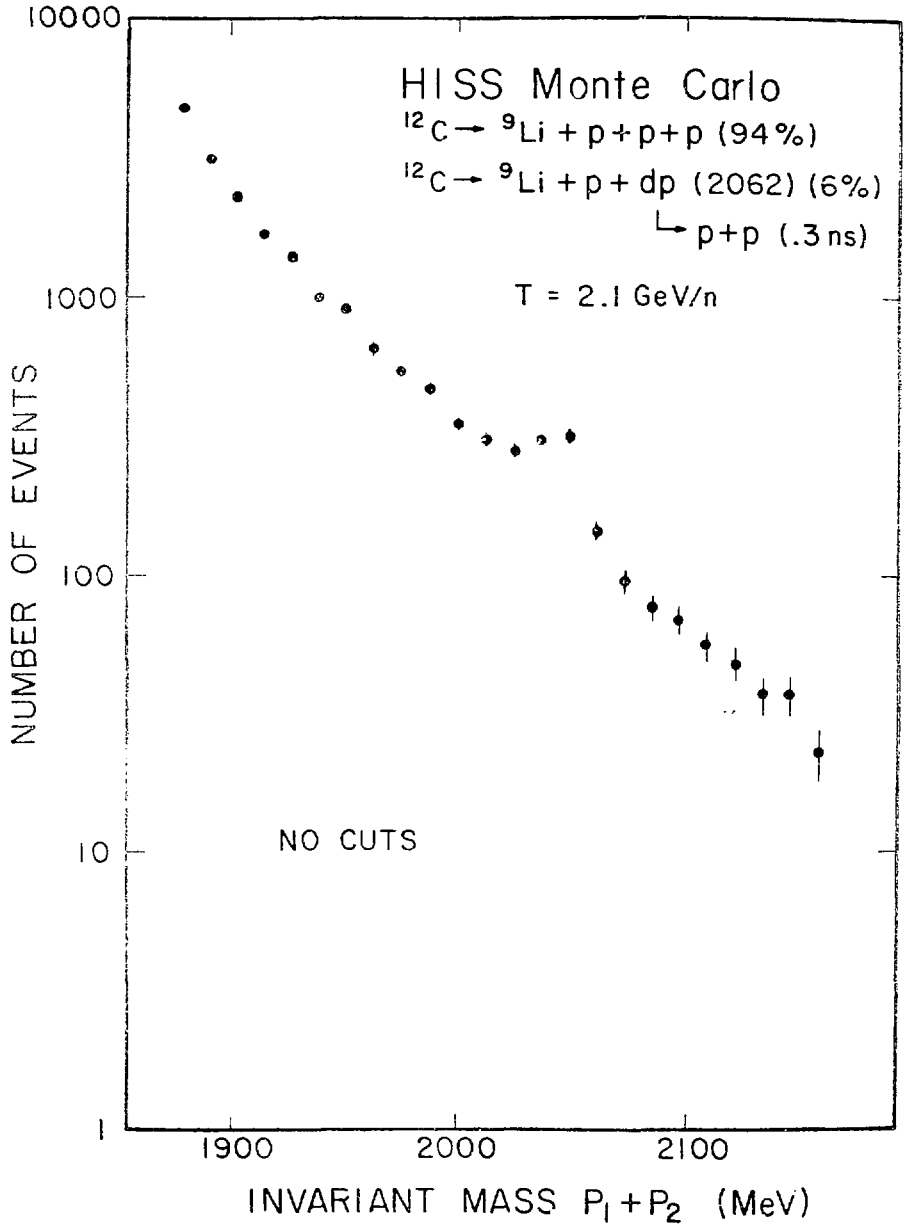
HISS Monte Carlo
$^{12}C \rightarrow {}^{9}Li + p + p + p$ (94%)
$^{12}C \rightarrow {}^{9}Li + p + dp$ (2062) (6%)
$\hookrightarrow p + p$ (.3 ns)
T = 2.1 GeV/n
NO CUTS
NUMBER OF EVENTS
INVARIANT MASS $P_1 + P_2$ (MeV)
10000
1000
100
10
1
1900
2000
2100

Figure 23.

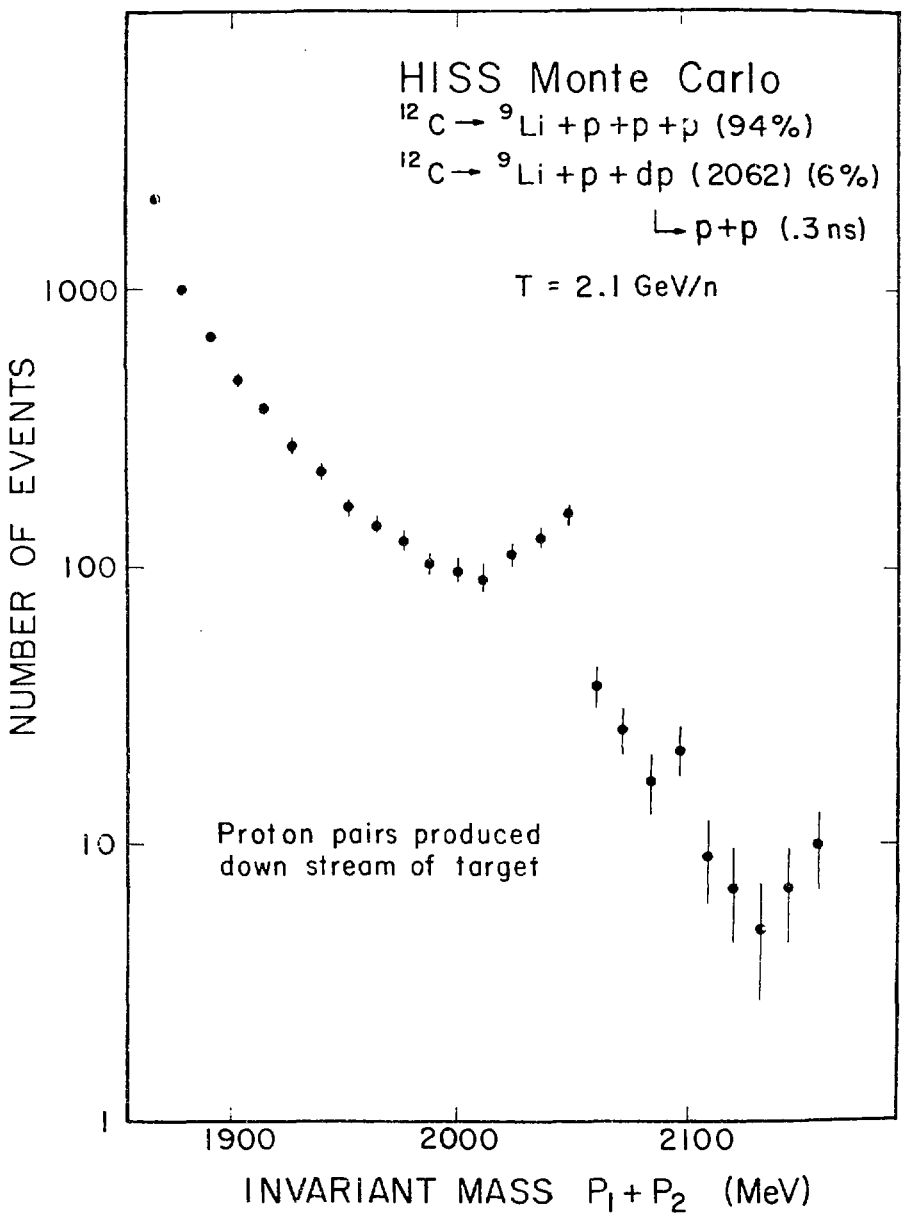
HISS Monte Carlo
$^{12}C \rightarrow {}^{9}Li + p + p + p$ (94%)
$^{12}C \rightarrow {}^{9}Li + p + dp$ (2062) (6%)
$\hookrightarrow p + p$ (.3 ns)
T = 2.1 GeV/n
Proton pairs produced
down stream of target
NUMBER OF EVENTS
1000
100
10
1
1900
2000
2100
INVARIANT MASS $P_1 + P_2$ (MeV)

Figure 24.

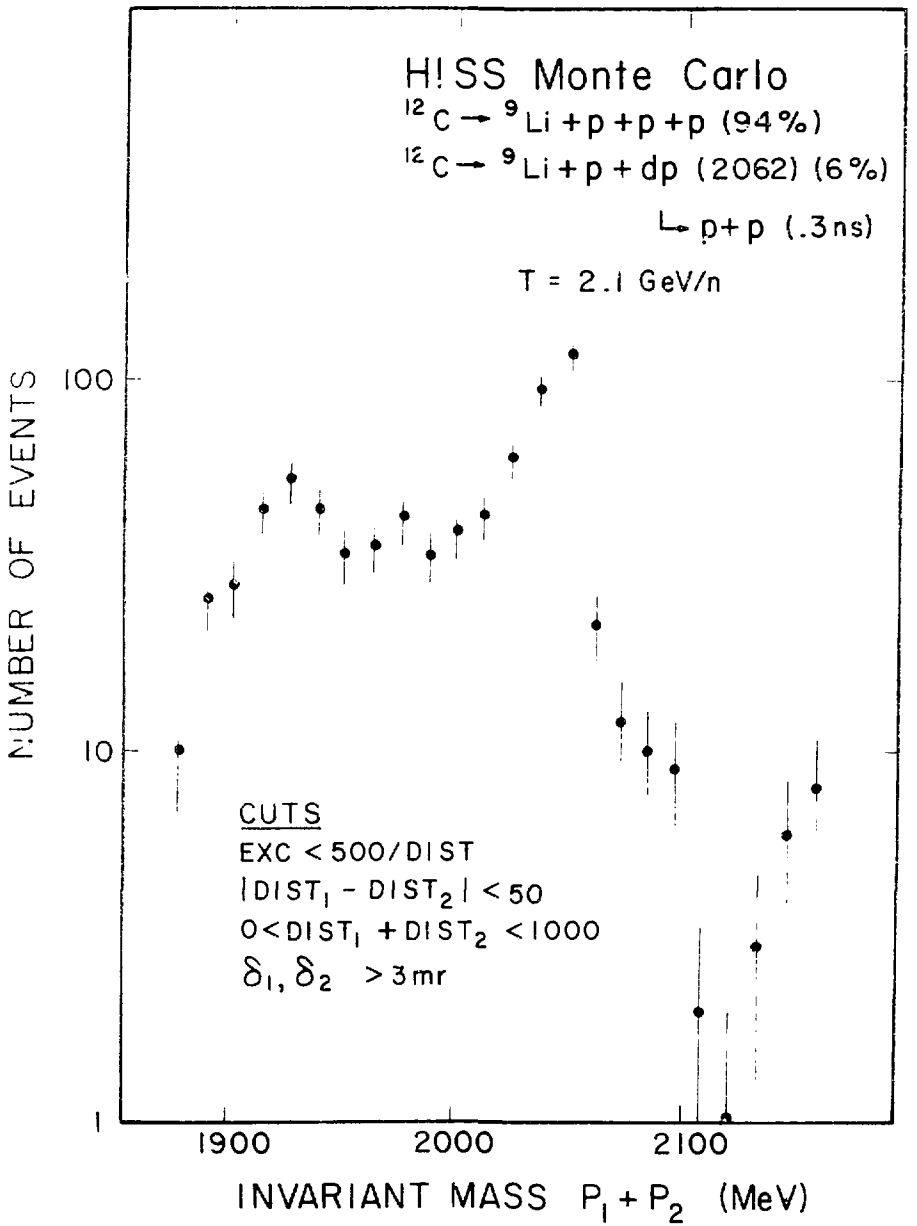
HISS Monte Carlo
$^{12}C \rightarrow {}^{9}Li + p + p + p$ (94%)
$^{12}C \rightarrow {}^{9}Li + p + dp$ (2062) (6%)
$\hookrightarrow p + p$ (.3ns)
T = 2.1 GeV/n
NUMBER OF EVENTS
100
10
1
CUTS
EXC < 500/DIST
$|DIST_1 - DIST_2| < 50$
$0 < DIST_1 + DIST_2 < 1000$
$\delta_1, \delta_2 > 3$mr
1900
2000
2100
INVARIANT MASS $P_1 + P_2$ (MeV)

Figure 25.